THE JOURNAL OF PHYSICAL CHEMISTRY Letters

pubs.acs.org/JPCL Letter

Water and Ion Transfer to Narrow Carbon Nanotubes: Roles of Exterior and Interior

Vadim Neklyudov and Viatcheslav Freger*

Cite This: *J. Phys. Chem. Lett.* 2021, 12, 185–190 Read Online

ACCESS | Metrics & More | Article Recommendations | Supporting Information

ABSTRACT: Narrow carbon nanotubes (CNTs) desalinate water, mimicking water channels of biological membranes, yet the physics behind selectivity, especially the effect of the membrane embedding CNTs on water and ion transfer, is still unclear. Here, we report *ab initio* analysis of the energies involved in transfer of water and K^+ and Cl^- ions from solution to empty and water-filled 0.68 nm CNTs for different dielectric constants (ϵ) of the surrounding matrix. The transfer energies computed for $1 \leq \epsilon < \infty$ permit a transparent breakdown of the transfer energy to three main contributions: binding to CNT, intra-CNT hydration, and dielectric polarization of the matrix. The latter scales inversely with ϵ and is of the order $10^2/\epsilon$ kJ/mol for both ions, which may change ion transfer from favorable to unfavorable, depending on ion, ϵ, and CNT diameter. This may have broad implications for designing and tuning selectivity of nanochannel-based devices.

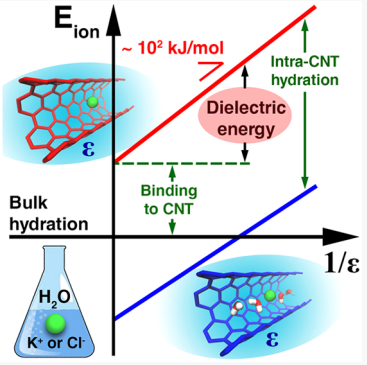

Downloaded via LAWRENCE LIVERMORE NATL LAB on July 31, 2022 at 01:44:40 (UTC).
See https://pubs.acs.org/sharingguidelines for options on how to legitimately share published articles.

Living cells desalinate water using specialized protein channels (aquaporins) embedded in cell membranes.[1] Inner channels of carbon nanotubes (CNTs) show much similarity with aquaporins, making CNT porins (CNTPs) attractive for next-generation water purification devices, as well as other bio- and nanotechnology applications.[2−4] Extensive experimental[5−9] and theoretical[10−14] studies shed light on intriguing mechanism of water flow via CNTs. In CNTs wider than about a nanometer, water displays essentially a bulk-like behavior.[6] However, similar to graphene nanoslits,[15] atomically smooth inner walls of narrow subnanometer CNTs minimize de Broglie scattering and allow an exceptionally fast single-file water transport at rates greatly exceeding hydrodynamic predictions.[6,16]

Narrow CNTs also exclude ions displaying selectivity on par with today's desalination membranes.[5,17] Charge repulsion by ionized groups at CNT rims or ions adsorbed on inner walls was suggested as a possible ion-exclusion mechanism.[5,6,8,10,18,19] Indeed, continuum models of charged nanochannels reasonably describe ion transport in wide CNTs that display a moderate selectivity.[8,18,20] Yet, high selectivity of subnanometer CNTPs apparently involves distinctly different physics and, in particular, dielectric exclusion, originating from polarization of the medium surrounding the ion.[17] This energy reduces compensation for ion dehydration upon transfer from bulk solution to CNT interior and raises transfer energy.[21−23] Nevertheless, despite recent progress,[24,25] understanding all contributions to the energy of ion transfer to narrow CNTs, including dielectric effects, is still incomplete.

A noteworthy point is that polarizing fields may readily cross the CNT walls and extend to CNT exterior. For instance, molecular dynamics (MD) simulations showed that a charge placed next to a CNT could stop water flow,[26] and even weaker dipolar interactions may similarly modulate it.[27] Simulations also find that the effect is reciprocal and water moving in the channel may drag along surrounding molecules.[28] These results strongly suggest that the medium around a CNT may affect its selectivity. Because, like aquaporins in cell membranes, CNTPs need to be embedded in an insulating host membrane or matrix, understanding the effect of such a matrix is crucial both for understanding the selectivity mechanism and for designing optimal CNTP-based systems. Here we investigate this aspect, which has not been examined systematically, focusing on the relation between the dielectric constant (ϵ) of the matrix hosting CNTPs and the transfer energies for water molecules and K^+ and Cl^- ions, for which data on cation−anion selectivity in CNTPs are available.[5] As the parametrization used in classical MD simulations might not capture intricacies of ion−water−CNT interactions,[16,29] we resort to computing the appropriate energies *ab initio*. Because our main interest is in the single-file arrangement, not always guaranteed in CNTs even as narrow as 0.8 nm,[24] we select 0.68 nm CNTs, about the narrowest ones to allow passage of water.[10]

Received: October 11, 2020
Accepted: December 7, 2020
Published: December 16, 2020

ACS Publications © 2020 American Chemical Society

https://dx.doi.org/10.1021/acs.jpclett.0c03093
J. Phys. Chem. Lett. 2021, 12, 185−190

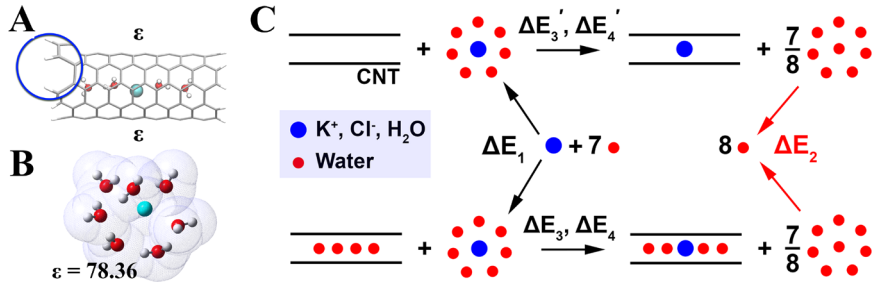

Figure 1. (A) Simulated cell cut out of optimized infinite CNT and terminated with hydrogen atoms. (B) Finite cluster of seven water molecules around the species of interest embedded in a dielectric continuum with ϵ = 78.36 simulating bulk hydration. The solvent-accessible surface is also shown. Gray, red, white, and cyan are carbon, oxygen, hydrogen atoms, and the species of interest (H_2O molecule, K^+ or Cl^- ions), respectively. (C) Thermodynamic cycles for computing transfer energies for different species between gas phase, bulk water, an empty CNT, and a water file within a CNT.

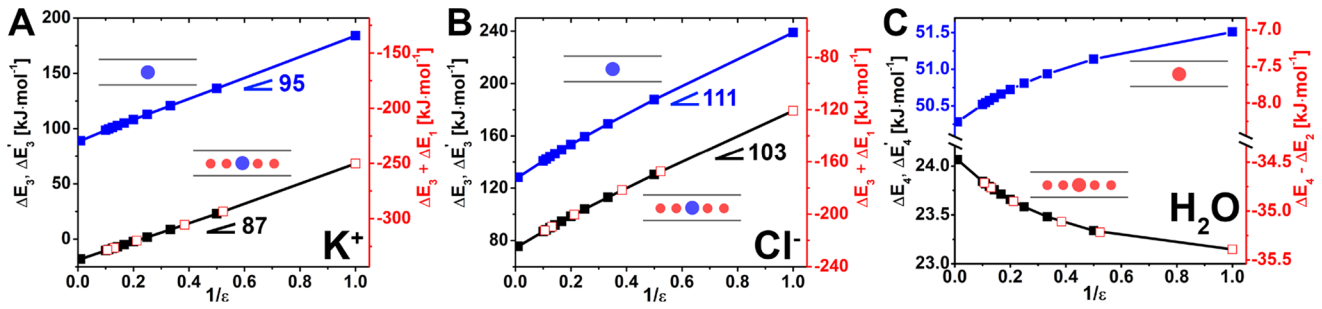

Figure 2. Variation of the transfer energies for K^+ (A) and Cl^- (B) ions and a water molecule (C) with $1/\epsilon$. The left and right vertical axes correspond to transfer from bulk water and from vacuum, respectively. Blue lines represent transfer of the respective ion ($\Delta E_3'$) or water molecule ($\Delta E_4'$) into an empty CNT. Black lines represent insertion of the respective ion (ΔE_3) or water molecule (ΔE_4) in water file within a CNT. Indicated are the slopes of the lines. The filled symbols are results computed for CNT embedded in a dielectric continuum. The empty red symbols represent CNT embedded (in the order of increasing ϵ) in vacuum and effective media representing common solvents (heptane, hexanoic acid, chloroform, iodoethane, and 2-bromopropane).

The analyzed cell was a (5,5) metallic CNT of length 1.73 nm and diameter 0.68 nm shown in Figure 1A. Its initial structure without or with water molecules and ions inside was first generated in SIESTA[30] at the PBE/DZP level under periodic boundary conditions, as part of an infinite CNT(5,5). The structure was optimized at 0 K, equilibrated using *ab initio* MD at 298.15 K; five different snapshots were then reoptimized, and the structure with the lowest energy was selected. It was also verified by varying the file length that a five species-long single file does not exert excessive internal stress, distorting the cylindrical symmetry of the optimized CNT cell. For subsequent calculations, a 1.73 nm long fragment was cut out and dangling bonds at the rims were terminated with hydrogens (Figure 1A). To facilitate computations, we employed B3LYP[31] approximation with 6-31G(d) basis implemented in *Gaussian 09*, rev. B.01.[32] The environment around CNT was simulated using the polarizable continuum model IEFPCM.[33] Bulk hydration energies were computed by optimizing the cluster of the species of interest surrounded by seven water molecules and embedded in a continuum with ϵ = 78.36 (Figure 1B). Previous studies and our computations (Figure S4 in the Supporting Information) showed that this cluster size reasonably represents bulk coordination for K^+ and Cl^- and well reproduces their hydration,[34−40] and it suits water as well.[41,42] The thermodynamic cycles used to derive transfer energies are schematically shown in Figure 1C. We first benchmarked energy computations versus experimental enthalpies of ion hydration ΔE_1 (transfer from vacuum to bulk water) and water vaporization ΔE_2, computed as follows:[42,43]

$$\Delta E_1 = E[X(H_2O)_7] - E[X] - 7(E[(H_2O)_8]/8) \quad (1)$$

$$\Delta E_2 = E[H_2O] - E[(H_2O)_8]/8 \quad (2)$$

where X = K^+ or Cl^-; single species (X or H_2O) are in vacuum, and corresponding clusters are embedded in a water-like continuum (Figure 1B). Note that the above relations approximate the respective excess free energies with enthalpies. This ignores excess entropies, which may be a significant factor in filling 0.8−1 nm CNTs with water;[44,45] however, in the present case, especially, for ion transfer, such entropic contributions would be fairly small compared to enthalpies and dielectric energy. The computed ΔE_1 = −318 kJ/mol for K^+ and ΔE_2 = 58 kJ/mol for water were reasonably close to respective experimental values, −334 and 44 kJ/mol.[46−48] For Cl^-, the computed ΔE_1 = −300 kJ/mol underestimated the experimental value −367 kJ/mol;[46] however, similar underestimates for Cl^- were found in other studies.[22,42] Apparently, the discrepancies reflect the level of theory, especially, unaccounted for dispersion correction. Indeed, we found that extended basis sets produced only a marginal difference, <5 kJ/mol, yet agreement much improved for the WB97XD functional[49] with Grimme's dispersion correction.[50] Nevertheless, such improvements insignificantly affected the dielectric energy, as expected from its long-range nature; therefore, faster computations were preferred (see Figures S4−S6 for more details).

To differentiate the interactions with CNT, dielectric energy, and intra-CNT hydration, we computed the transfer energies for two scenarios: (I) insertion of the species into a

https://dx.doi.org/10.1021/acs.jpclett.0c03093
J. Phys. Chem. Lett. 2021, 12, 185−190

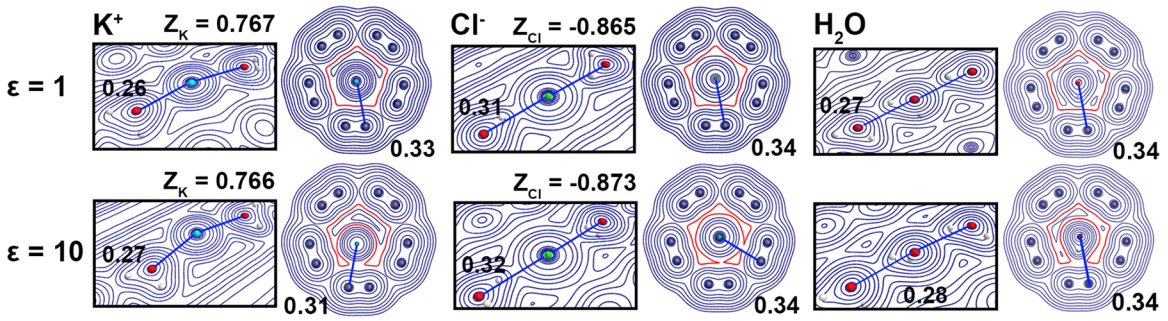

Figure 3. Electron density distribution along and across CNT around hydrated K^+, Cl^-, and H_2O for $\epsilon = 1$ (top row) and $\epsilon = 10$ (bottom row). The numbers within the maps are indicated distances in nanometers. Z_K and Z_{Cl} are residual ion charges.

water file within CNTP and (II) transfer of a single species to an empty CNTP. In scenario I, we presumed that proximity to a water file terminus ("surface energy" of the file, *ca.* 17 kJ/mol, see the Supporing Information) substantially affects only two terminal molecules at each terminus. We then approximated solvation in a long file by that in the middle position of a 5-member file. For both scenarios the transfer energies, ΔE_3 for ions and ΔE_4 for water, were then computed as follows (Figure 1C):

$$\Delta E_3 = E[\mathrm{X(H_2O)_4\ in\ CNT}] + 7(E[(\mathrm{H_2O})_8]/8) - E[(\mathrm{H_2O})_4\ \mathrm{in\ CNT}] - E[\mathrm{X(H_2O)_7}] \quad (3)$$

$$\Delta E_4 = E[(\mathrm{H_2O})_5\ \mathrm{in\ CNT}] - E[(\mathrm{H_2O})_8]/8 - E[(\mathrm{H_2O})_4\ \mathrm{in\ CNT}] \quad (4)$$

In all initial and final states, the CNT was embedded in a dielectric continuum with a corresponding ϵ. Scenario I was addressed by considering the four terminal water molecules as real molecules (energies ΔE_3 and ΔE_4), whereas in scenario II (energies $\Delta E_3'$ and $\Delta E_4'$) they were noninteracting dummy molecules that excluded the external continuum and kept $\epsilon = 1$ inside the CNT.

Panels A and B in Figure 2 display the key result, the ion transfer energies ΔE_3 (water-filled channel, black lines) and $\Delta E_3'$ (empty tube, blue lines) plotted versus $1/\epsilon$. Here, the zero energy corresponds to ion bulk dehydration, $-\Delta E_1'$, different for each species. Empty symbols are results for the dielectric continuum around CNT replaced with effective media representing various common solvents and including various *ad hoc* corrections for solvent-specific short-range non-dispersive interactions (hydrogen bond acidity and basicity, aromaticity, and electronegative halogenicity). The fact that *ad hoc* media closely match the trend of dielectric continua indicates that ϵ of the exterior is the main factor controlling its interaction with the ion. This could be expected, as CNT walls efficiently eliminate specific short-range interactions. For both ions, ΔE_3 and $\Delta E_3'$ show similar linear dependence with slopes of the order 10^2 kJ/mol, only slightly different for each ion and scenario. The linear dependence on $1/\epsilon$ is suggested by the Born solvation energy of an ion in a dielectric continuum

$$E_{\mathrm{Born}} = \frac{e^2}{8\pi\epsilon_0\epsilon R} \quad (5)$$

where e is the electron charge, ϵ_0 the permittivity of vacuum, and R the effective radius of an equivalent ideally polarizable spherical cavity containing the ion, identified as the ion radius in the simple theory.

In contrast to previous computations of transfer energies for a specific surrounding (usually, vacuum $\epsilon = 1$ or a lipid membrane $\epsilon \approx 2$), the entire dependence of ΔE_3 and $\Delta E_3'$ on $1/\epsilon$ obtained here permits a transparent breakdown of the transfer energy to distinct contributions. Specifically, it differentiates the dielectric energy of the exterior from intra-CNT interactions. Indeed, the exterior polarization vanishes for $1/\epsilon = 0$ ($\epsilon = \infty$); therefore, the intercept of $\Delta E_3'$ (the leftmost point on the blue line) reflects only ion binding to bare CNT relative to its dehydration energy, $-\Delta E_1$. It is about 89 kJ/mol for K^+ and 128 kJ/mol for Cl^- in present computations, and the increase of $\Delta E_3'$ above this value for finite ϵ, varying about linearly with $1/\epsilon$ (eq 5), represents the dielectric polarization of the exterior. This contribution substantially increases the transfer energy, reaching its maximum, about +184 kJ/mol for K^+ and +239 kJ/mol for Cl^-, at $\epsilon = 1$ (vacuum). Finally, the vertical separation of the black and blue lines, $\Delta E_3 - \Delta E_3'$, is the energy of the intra-CNT ion hydration. Although it is only a fraction of the bulk hydration, it is commensurate with the other contributions and substantially offsets the dehydration penalty.

To appreciate the relative role of different contributions, consider $\epsilon = 2$, typical of lipid membranes.[51] The total transfer energy for K^+ ion, 23 kJ/mol, is made up of 89 (ion binding to CNT relative to bulk hydration), −113 (intra-CNT hydration), and +47 kJ/mol (dielectric energy). For Cl^-, the respective values sum up as +130 = 128 − 58 + 60 kJ/mol. Although the absolute numbers may change with the level of theory, it is seen that the dielectric energy for K^+ is commensurate with the other contributions; therefore, potassium transfer to CNT may be both favorable and unfavorable, depending on ϵ. The insertion of Cl^- in a water-filled CNTP has a positive energy penalty at any ϵ value; however, increasing the dielectric constant can significantly reduce it.

Note that, on the basis of eq 5, the linear slopes in Figure 2A,B may be identified as $e^2/8\pi\epsilon_0 R_{\mathrm{ef}}$ with some effective value of R_{ef}. They yield $R_{\mathrm{ef}} = 0.73$ nm for K^+ and $R_{\mathrm{ef}} = 0.62$ nm for Cl^-, which significantly exceeds and does not match the order of the respective bare ion radii R_{ion}, 0.141 and 0.180 nm.[52] The difference between R_{ef} and R_{ion} reflects the CNT electron cloud polarization by the ion as well as ion charge delocalization due to ion bonding with CNT. Apparently, the smaller K^+ more strongly binds to CNT, resulting in larger R_{ef}, compared to Cl^-. The fact that R_{ef} is intermediate to the CNT radius (0.34 nm) and half-length (0.865 nm) suggests

https://dx.doi.org/10.1021/acs.jpclett.0c03093
J. Phys. Chem. Lett. 2021, 12, 185−190

that polarization and charge delocalization extend along the entire CNT, distorting spherical symmetry and reducing intensity of the ion field. The small difference between the slopes of ΔE_3 and $\Delta E_3'$ indicates an additional weak polarization of water within water-filled CNT, which slightly increases R_{ef} to 0.79 and 0.63 nm, respectively.

The above effects may be more explicitly observed in electron density maps in Figure 3 and, specifically, the interatomic distances and the residual ion charge Z_{ion} evaluated in GAUSSIAN using the natural bond orbital analysis.[53] K^+ shows stronger binding and charge delocalization, manifested in a smaller residual charge, $Z_K \approx +0.77$, and shorter K−C distance, compared with $Z_{Cl} \approx -0.87$ and Cl−C distance. Notably, the maps for $\epsilon = 1$ and $\epsilon = 10$ indicate that, at higher ϵ, K^+ bonds more strongly to CNT and more weakly interacts with water (*cf.* longer ion−water oxygen distance), which is less pronounced for Cl^- and consistent with its smaller R_{ef}.

Compared to ions, transfer energies for H_2O ΔE_4 and $\Delta E_4'$ (Figure 2C) show a much weaker dependence on ϵ, as expected of a dipole. While the decreasing trend of $\Delta E_4'$ versus $1/\epsilon$ is reminiscent of ions' $\Delta E_3'$, it reverses for ΔE_4. The difference $\Delta E_4 - \Delta E_4'$ reflects the water−water interaction, slightly weakened at higher ϵ. This is also observed in electron density maps in Figure 3 as the larger distance between water oxygens and weaker bonding at $\epsilon = 10$, relative to $\epsilon = 1$. Ultimately, in contrast to ions, water transfer to CNTs is somewhat promoted rather than impeded by a lower-dielectric surrounding.

As explained before, the present choice of 0.68 nm nanotubes, presumably the narrowest permeable,[10] was to ensure the single-file arrangement, but the experimental data for this diameter are unavailable. Because 0.8 nm CNTPs may still preserve or only partly distort the single file, some trends should be qualitatively similar to 0.68 nm channels. Indeed, reversal potential measurements in 0.8 nm CNTPs indicate a K:Cl selectivity *ca.* 200:1,[5] which is fully consistent with the far more favorable transfer energy of K^+ vs Cl^- found here. Similarly, water transfer is more favorable compared to Cl^-, the ion that has the larger transfer energy and controls salt transfer, *i.e.* CNTPs should desalinate water, as observed for 0.8 nm tubes.[5] We anticipate that in wider tubes water−water interaction within the file, $\Delta E_4' - \Delta E_4 \approx -28$ kJ/mol, should not change significantly, but short-range dipolar interactions of water with CNT (ΔE_4) may weaken, further facilitating water transfer.

On the other hand, increased CNT diameter may oppositely affect ion transfer in 0.8 nm nanotubes. Specifically, R_{ef} should about linearly correlate with the CNT diameter. The 15% difference between 0.68 and 0.8 nm CNTs may then reduce the dielectric energy, inversely related to R_{ef}, by up to 15 kJ/mol depending on ϵ. It is more speculative to project to wider channels the ion−CNT interaction; yet, if they are viewed as adsorption on inner walls, the biding energy is expected to scale roughly as the surface area per CNT volume, *i.e.*, about inversely depend on the CNT diameter, similar to dielectric energy. As an illustration, we may project the present data for 0.68 nm to 0.8 nm CNTPs embedded in a lipid bilayer of dielectric constant 2.4[54] and estimate transfer energies for water and Cl^-, as follows. For water, intra-CNT hydration and bulk dehydration are −28 and 58 kJ/mol, respectively; therefore, partial dehydration within CNT costs −28 + 58 = 30 kJ/mol. Binding of a water molecule from vacuum to bare 0.68 nm CNT amounts to $\Delta E_4' - \Delta E_2 \approx -8$ kJ/mol (see the right axis in Figure 2C). With insignificant dielectric energy, the dehydration energy unchanged, and the binding energy from vacuum reduced by 15%, water transfer energy to 0.8 nm CNTPs would be about 23 kJ/mol. This matches well experimental transport activation energies (22 kJ/mol) as well as *ab initio* computations (20 kJ/mol).[25]

For Cl^- and $\epsilon = 2.4$, the computed intra-CNT hydration energy $\Delta E_3' - \Delta E_3 \approx -60$ kJ/mol versus bulk dehydration 300 kJ/mol may stay unchanged in 0.8 nm CNTP, while ion binding from vacuum $\Delta E_3' + \Delta E_1 \approx -172$ (right axis in Figure 2B for $1/\epsilon = 0$) and dielectric energy 111/2.4 = 46 kJ/mol are to be reduced by 15%. Ultimately, this yields the transfer energy 137 kJ/mol. This significantly exceeds the reported experimental activation barrier for Cl^-, 52 kJ/mol.[25] The same report states that this value matched a theoretical value 63 kJ/mol computed using a hybrid DFT method. However, their simulations artificially placed highly polarizable graphene sheets at the CNT exterior, which could produce a situation, equivalent to a large ϵ in the present model. This amounts to discarding 46 kJ/mol of dielectric energy, which would take their result close to the present estimate. As an alternative explanation, we speculate that the discrepancy might point to a distortion of single water file around Cl^-. Indeed, our preliminary results indicate that Cl^- in the 0.8 nm (6,6) CNT is solvated by three rather than two water molecules (see Figure S7), which should decrease transfer energy by several tens of kilojoules per mole. Examination of this point using a higher level of theory for Cl^- and other ions is currently underway, but it is well in line with a similar result reported for small cations in 0.8 CNTPs.[24]

In summary, the present approach, analyzing the variation of the transfer energy in the entire range $1 \leq \epsilon < \infty$, permits a transparent breakdown of the water and ion transfer energies to several distinct contributions. Along with ion-specific effects that favor uptake of K^+ vs Cl^- ions, the analysis highlights the significance of ion interactions with the matrix surrounding the CNT, controlled by its dielectric constant ϵ. The latter contribution is of the order of a few tens to a hundred kilojoules per mole for 0.68 nm CNTs, which may change ion transfer from favorable to unfavorable in response to decreasing ϵ. It is expected to remain substantial in wider nanotubes, as long as they preserve the single-file water arrangement, though the effect of weaker binding on transport and water−ion selectivity may be more significant. The present results add to the general physical picture of dielectric exclusion as a key selectivity mechanism in desalination membranes and nanochannels.

■ ASSOCIATED CONTENT

Supporting Information

The Supporting Information is available free of charge at https://pubs.acs.org/doi/10.1021/acs.jpclett.0c03093.

Procedure for building model structures, details of quantum-chemical calculations in a SIESTA; examination of the effect of water and ion/water clusters size and level of theory on computed hydration enthalpies, free energies, and the dielectric energy; the estimations of the "surface energy" of a water file terminus; and the optimized structure of hydrated chloride ion in CNT-(6,6) (PDF)

https://dx.doi.org/10.1021/acs.jpclett.0c03093
J. Phys. Chem. Lett. 2021, 12, 185−190

AUTHOR INFORMATION

Corresponding Author

Viatcheslav Freger − *Wolfson Department of Chemical Engineering, Technion - IIT, Haifa 32000, Israel; Russel Berrie Nanotechnology Institute and Grand Technion Energy Program, Technion - IIT, Haifa 32000, Israel;* orcid.org/0000-0001-8067-052X; Phone: +972 (0) 4 829 2933; Email: vfreger@technion.ac.il

Author

Vadim Neklyudov − *Wolfson Department of Chemical Engineering, Technion - IIT, Haifa 32000, Israel*

Complete contact information is available at: https://pubs.acs.org/10.1021/acs.jpclett.0c03093

Notes

The authors declare no competing financial interest.

ACKNOWLEDGMENTS

The financial support by a joint grant 2016627 from the United States-Israel Binational Science Foundation (Israel) and National Science Foundation (United States) and by the Planning & Budgeting Committee, Israel Council for Higher Education and Fuel Choice Initiative (Prime Minister Office of Israel) within the framework of "Israel National Research Center for Electrochemical Propulsion (INREP)" is acknowledged. The authors thank Aleksandr Noy and Meni Wanunu for discussions and many valuable suggestions.

REFERENCES

(1) Agre, P.; King, L. S.; Yasui, M.; Guggino, W. B.; Ottersen, O. P.; Fujiyoshi, Y.; Engel, A.; Nielsen, S. Aquaporin water channels−from atomic structure to clinical medicine. *J. Physiol.* **2002**, *542*, 3−16.

(2) Dittrich, P. S.; Manz, A. Lab-on-a-chip: microfluidics in drug discovery. *Nat. Rev. Drug Discovery* **2006**, *5*, 210−218.

(3) Ghosh, S.; Sood, A.; Kumar, N. Carbon nanotube flow sensors. *Science* **2003**, *299*, 1042−1044.

(4) Chaban, V. V.; Prezhdo, O. V. Water boiling inside carbon nanotubes: toward efficient drug release. *ACS Nano* **2011**, *5*, 5647−5655.

(5) Tunuguntla, R. H.; Henley, R. Y.; Yao, Y.-C.; Pham, T. A.; Wanunu, M.; Noy, A. Enhanced water permeability and tunable ion selectivity in subnanometer carbon nanotube porins. *Science* **2017**, *357*, 792−796.

(6) Holt, J. K.; Park, H. G.; Wang, Y.; Stadermann, M.; Artyukhin, A. B.; Grigoropoulos, C. P.; Noy, A.; Bakajin, O. Fast mass transport through sub-2-nanometer carbon nanotubes. *Science* **2006**, *312*, 1034−1037.

(7) Hinds, B.; Chopra, N.; Rantell, T.; Andrews, R. Aligned multiwalled carbon nanotube membranes. *Science* **2004**, *303*, 62−65.

(8) Secchi, E.; Niguès, A.; Jubin, L.; Siria, A.; Bocquet, L. Scaling behavior for ionic transport and its fluctuations in individual carbon nanotubes. *Phys. Rev. Lett.* **2016**, *116*, 154501.

(9) Majumder, M.; Chopra, N.; Andrews, R.; Hinds, B. Enhanced flow in carbon nanotubes. *Nature* **2005**, *438*, 44−44.

(10) Corry, B. Designing carbon nanotube membranes for efficient water desalination. *J. Phys. Chem. B* **2008**, *112*, 1427−1434.

(11) Hummer, G.; Rasaiah, J.; Noworyta, J. Water conduction through the hydrophobic channel of a carbon nanotube. *Nature* **2001**, *414*, 188−190.

(12) Striolo, A. The mechanism of water diffusion in narrow carbon nanotubes. *Nano Lett.* **2006**, *6*, 633−639.

(13) Won, C. Y.; Joseph, S.; Aluru, N. R. Effect of quantum partial charges on the structure and dynamics of water in single-walled carbon nanotubes. *J. Chem. Phys.* **2006**, *125*, 114701.

(14) Chaban, V. V.; Prezhdo, V. V.; Prezhdo, O. V. Confinement by carbon nanotubes drastically alters the boiling and critical behavior of water droplets. *ACS Nano* **2012**, *6*, 2766−2773.

(15) Keerthi, A.; Geim, A.; Janardanan, A.; Rooney, A.; Esfandiar, A.; Hu, S.; Dar, S.; Grigorieva, I.; Haigh, S.; Wang, F.; Radha, B. Ballistic molecular transport through twodimensional channels. *Nature* **2018**, *558*, 420−424.

(16) Kalra, A.; Garde, S.; Hummer, G. Osmotic water transport through carbon nanotube membranes. *Proc. Natl. Acad. Sci. U. S. A.* **2003**, *100*, 10175−10180.

(17) Freger, V. Selectivity and polarization in water channel membranes: lessons learned from polymeric membranes and CNTs. *Faraday Discuss.* **2018**, *209*, 371−388.

(18) Fornasiero, F.; Park, H. G.; Holt, J. K.; Stadermann, M.; Grigoropoulos, C. P.; Noy, A.; Bakajin, O. Ion exclusion by sub-2-nm carbon nanotube pores. *Proc. Natl. Acad. Sci. U. S. A.* **2008**, *105*, 17250−17255.

(19) Grosjean, B.; Pean, C.; Siria, A.; Bocquet, L.; Vuilleumier, R.; Bocquet, M.-L. Chemisorption of hydroxide on 2D materials from DFT calculations: graphene versus hexagonal boron nitride. *J. Phys. Chem. Lett.* **2016**, *7*, 4695−4700.

(20) Biesheuvel, P. M.; Bazant, M. Z. Analysis of ionic conductance of carbon nanotubes. *Phys. Rev. E: Stat. Phys., Plasmas, Fluids, Relat. Interdiscip. Top.* **2016**, *94*, No. 050601.

(21) Epsztein, R.; DuChanois, R. M.; Ritt, C. L.; Noy, A.; Elimelech, M. Towards singlespecies selectivity of membranes with subnanometre pores. *Nat. Nanotechnol.* **2020**, *15*, 426.

(22) Li, Z.; Li, Y.; Yao, Y.-C.; Aydin, F.; Zhan, C.; Chen, Y.; Elimelech, M.; Pham, T. A.; Noy, A. Strong Differential Monovalent Anion Selectivity in Narrow Diameter Carbon Nanotube Porins. *ACS Nano* **2020**, *14*, 6269−6275.

(23) Song, C.; Corry, B. Intrinsic ion selectivity of narrow hydrophobic pores. *J. Phys. Chem. B* **2009**, *113*, 7642−7649.

(24) Zhan, C.; Aydin, F.; Schwegler, E.; Noy, A.; Pham, T. A. Understanding Cation Selectivity in Carbon Nanopores with Hybrid First-Principles/Continuum Simulations: Implications for Water Desalination and Separation Technologies. *ACS Appl. Nano Mater.* **2020**, *3*, 9740.

(25) Li, Y.; Li, Z.; Aydin, F.; Quan, J.; Chen, X.; Yao, Y.-C.; Zhan, C.; Chen, Y.; Pham, T. A.; Noy, A. Water-ion permselectivity of narrow-diameter carbon nanotubes. *Sci. Adv.* **2020**, *6*, eaba9966.

(26) Li, J.; Gong, X.; Lu, H.; Li, D.; Fang, H.; Zhou, R. Electrostatic gating of a nanometer water channel. *Proc. Natl. Acad. Sci. U. S. A.* **2007**, *104*, 3687−3692.

(27) Gong, X.; Li, J.; Zhang, H.; Wan, R.; Lu, H.; Wang, S.; Fang, H. Enhancement of water permeation across a nanochannel by the structure outside the channel. *Phys. Rev. Lett.* **2008**, *101*, 257801.

(28) Wang, B.; Kral, P. Coulombic dragging of molecules on surfaces induced by separately flowing liquids. *J. Am. Chem. Soc.* **2006**, *128*, 15984−15985.

(29) Liu, L.; Patey, G. Simulated conduction rates of water through a (6, 6) carbon nanotube strongly depend on bulk properties of the model employed. *J. Chem. Phys.* **2016**, *144*, 184502.

(30) Soler, J. M.; Artacho, E.; Gale, J.; Garc, A.; et al. The SIESTA method for ab initio order-N materials simulation. *J. Phys.: Condens. Matter* **2002**, *14*, 2745.

(31) Lee, C.; Yang, W.; Parr, R. G. Development of the Colle-Salvetti correlation-energy formula into a functional of the electron density. *Phys. Rev. B: Condens. Matter Mater. Phys.* **1988**, *37*, 785.

(32) Frisch, M. J.; Trucks, G. W.; Schlegel, H. B.; Scuseria, G. E.; Robb, M. A.; Cheeseman, J. R.; Scalmani, G.; Barone, V.; Mennucci, B.; Petersson, G. A.; Nakatsuji, H.; Caricato, M.; Li, X.; Hratchian, H. P.; Izmaylov, A. F.; Bloino, J.; Zheng, G.; Sonnenberg, J. L.; Hada, M.; Ehara, M.; Toyota, K.; Fukuda, R.; Hasegawa, J.; Ishida, M.; Nakajima, T.; Honda, Y.; Kitao, O.; Nakai, H.; Vreven, T.; Montgomery, J. A.; Peralta, J. E.; Ogliaro, F.; Bearpark, M.; Heyd, J. J.; Brothers, E.; Kudin, K. N.; Staroverov, V. N.; Kobayashi, R.; Normand, J.; Raghavachari, K.; Rendell, A.; Burant, J. C.; Iyengar, S. S.; Tomasi, J.; Cossi, M.; Rega, N.; Millam, J. M.; Klene, M.; Knox, J.

E.; Cross, J. B.; Bakken, V.; Adamo, C.; Jaramillo, J.; Gomperts, R.; Stratmann, R. E.; Yazyev, O.; Austin, A. J.; Cammi, R.; Pomelli, C.; Ochterski, J. W.; Martin, R. L.; Morokuma, K.; Zakrzewski, V. G.; Voth, G. A.; Salvador, P.; Dannenberg, J. J.; Dapprich, S.; Daniels, A. D.; Farkas, O.; Foresman, J. B.; Ortiz, J. V.; Cioslowski, J.; Fox, D. J. *Gaussian 09*, revision B.01; 2009.

(33) Tomasi, J.; Mennucci, B.; Cances, E. The IEF version of the PCM solvation method: an overview of a new method addressed to study molecular solutes at the QM ab initio level. *J. Mol. Struct.: THEOCHEM* **1999**, *464*, 211−226.

(34) Mähler, J.; Persson, I. A study of the hydration of the alkali metal ions in aqueous solution. *Inorg. Chem.* **2012**, *51*, 425−438.

(35) Mancinelli, R.; Botti, A.; Bruni, F.; Ricci, M. A.; Soper, A. K. Hydration of sodium, potassium, and chloride ions in solution and the concept of structure maker/breaker. *J. Phys. Chem. B* **2007**, *111*, 13570−13577.

(36) Rao, J. S.; Dinadayalane, T. C.; Leszczynski, J.; Sastry, G. N. Comprehensive study on the solvation of mono-and divalent metal cations: Li^+, Na^+, K^+, Be^{2+}, Mg^{2+} and Ca^{2+}. *J. Phys. Chem. A* **2008**, *112*, 12944−12953.

(37) Zhu, F.; Zhou, H.; Zhou, Y.; Miao, J.; Fang, C.; Fang, Y.; Sun, P.; Ge, H.; Liu, H. The investigation of structure and IR spectra for hydrated potassium ion clusters $K^+(H_2O)$ n = 1−16 by density functional theory. *Eur. Phys. J. D* **2016**, *70*, 246.

(38) Robertson, W. H.; Johnson, M. A. Molecular aspects of halide ion hydration: The cluster approach. *Annu. Rev. Phys. Chem.* **2003**, *54*, 173−213.

(39) Bankura, A.; Santra, B.; DiStasio, R. A., Jr; Swartz, C. W.; Klein, M. L.; Wu, X. A systematic study of chloride ion solvation in water using van der Waals inclusive hybrid density functional theory. *Mol. Phys.* **2015**, *113*, 2842−2854.

(40) Bajaj, P.; Riera, M.; Lin, J. K.; Mendoza Montijo, Y. E.; Gazca, J.; Paesani, F. Halide Ion Microhydration: Structure, Energetics, and Spectroscopy of Small Halide−Water Clusters. *J. Phys. Chem. A* **2019**, *123*, 2843−2852.

(41) Li, F.; Wang, L.; Zhao, J.; Xie, J. R. H.; Riley, K. E.; Chen, Z. What is the best density functional to describe water clusters: Evaluation of widely used density functionals with various basis sets for (H_2O)n (n = 1−10). *Theor. Chem. Acc.* **2011**, *130*, 341−352.

(42) Mejıas, J.; Lago, S. Calculation of the absolute hydration enthalpy and free energy of H^+ and OH^-. *J. Chem. Phys.* **2000**, *113*, 7306−7316.

(43) Uudsemaa, M.; Tamm, T. Calculation of hydration enthalpies of aqueous transition metal cations using two coordination shells and central ion substitution. *Chem. Phys. Lett.* **2004**, *400*, 54−58.

(44) Pascal, T. A.; Goddard, W. A.; Jung, Y. Entropy and the driving force for the filling of carbon nanotubes with water. *Proc. Natl. Acad. Sci. U. S. A.* **2011**, *108*, 11794−11798.

(45) Waghe, A.; Rasaiah, J. C.; Hummer, G. Entropy of single-file water in (6,6) carbon nanotubes. *J. Chem. Phys.* **2012**, *137*, No. 044709.

(46) Marcus, Y. *Ions in Solution and their Solvation*; John Wiley & Sons, 2015.

(47) Medvedev, V.A.; Cox, J.D.; Wagman, D.D. *CODATA key values for thermodynamics*; Hemisphere Publishing Corporation: New York, 1989.

(48) Ben-Naim, A.; Marcus, Y. Solvation thermodynamics of nonionic solutes. *J. Chem. Phys.* **1984**, *81*, 2016−2027.

(49) Chai, J.-D.; Head-Gordon, M. Long-range corrected hybrid density functionals with damped atom−atom dispersion corrections. *Phys. Chem. Chem. Phys.* **2008**, *10*, 6615−6620.

(50) Grimme, S.; Antony, J.; Ehrlich, S.; Krieg, H. A consistent and accurate ab initio parametrization of density functional dispersion correction (DFT-D) for the 94 elements H-Pu. *J. Chem. Phys.* **2010**, *132*, 154104.

(51) Dilger, J. P.; McLaughlin, S.; McIntosh, T. J.; Simon, S. A. The dielectric constant of phospholipid bilayers and the permeability of membranes to ions. *Science* **1979**, *206*, 1196−1198.

(52) Marcus, Y. Ionic radii in aqueous solutions. *Chem. Rev.* **1988**, *88*, 1475−1498.

(53) Glendening, E.; Reed, A.; Carpenter, J. F. Weinhold, Inc.: Pittsburgh, PA, 2003.

(54) Dols-Perez, A.; Gramse, G.; Calo, A.; Gomila, G.; Fumagalli, L. Nanoscale electric polarizability of ultrathin biolayers on insulating substrates by electrostatic force microscopy. *Nanoscale* **2015**, *7*, 18327−18336.

https://dx.doi.org/10.1021/acs.jpclett.0c03093
J. Phys. Chem. Lett. 2021, 12, 185−190